ADVANCED MATERIALS
www.advmat.de

Enhanced SWIR Light Detection in Organic Semiconductor Photodetectors through Up-Conversion of Mid-Gap Trap States

Stefan Zeiske, Nasim Zarrabi, Oskar J. Sandberg, Sam Gielen, Wouter Maes, Paul Meredith,* and Ardalan Armin**

Shortwave-infrared (SWIR) photodetectors are vital for many scientific and industrial applications including surveillance, quality control and inspection. In recent decades, photodetectors based on organic semiconductors have emerged, demonstrating potential to add real value to broadband and narrowband imaging and sensing scenarios, where factors such as thermal budget sensitivity, large area aperture necessity, cost considerations, and lightweight and conformal flexibility demands are prioritized. It is now recognized that the performance of organic photodetectors (OPDs), notably their specific detectivity, is ultimately limited by trap states, universally present in disordered semiconductors. This work adopts an approach of utilizing these mid-gap states to specifically create a SWIR photo-response. To this end, this work introduces a somewhat counter-intuitive approach of "trap-doping" in bulk heterojunction (BHJs) photodiodes, where small quantities of a guest organic molecule are intentionally incorporated into a semiconducting donor:acceptor host system. Following this approach, this work demonstrates a proof-of-concept for a visible-to-SWIR broadband OPD, approaching (and, to some extent, even exceeding) state-of-the-art performance across critical photodetector metrics. The trap-doping approach is, even though only a proof-of-concept currently, broadly applicable to various spectral windows. It represents a new modality for engineering photodetection using the unconventional strategy of turning a limitation into a feature.

1. Introduction

Photodetection across the ultraviolet (UV) to the shortwave-infrared (SWIR; normally defined as ≈1.3 to ≈2.5 µm) spectral range is crucial for scientific and industrial applications, including (bio-)sensing and imaging,[1–5] machine vision,[6] and communication.[7–11] Over the past few decades, devices based on next-generation, organic semiconductors have emerged showing potential for UV-SWIR broadband and narrowband imaging and photodetection. Organic photodetectors (OPDs) present a compelling alternative to the state-of-the-art plethora of current technology which is largely based upon Silicon (Si), Germanium (Ge), and III-V semiconductor compounds like Indium Gallium Arsenide (InGaAs). While OPDs currently display inferior specific detectivities (D^*), compared to conventional technologies, there are several complementary scenarios where OPDs could prove valuable, especially for SWIR and broadband detection (spanning the VIS to SWIR).[12] These scenarios prioritize

S. Zeiske, N. Zarrabi, O. J. Sandberg, P. Meredith, A. Armin
Sustainable Advanced Materials (Sêr-SAM)
Centre for Integrative Semiconductor Materials and Department of Physics
Swansea University Bay Campus
Fabian Way, Swansea SA1 8EN, UK
E-mail: oskar.sandberg@abo.fi; paul.meredith@swansea.ac.uk; ardalan.armin@swansea.ac.uk

S. Zeiske
Department of Chemistry
Northwestern University
2145 Sheridan Rd, Evanston, IL 60208, USA

The ORCID identification number(s) for the author(s) of this article can be found under https://doi.org/10.1002/adma.202405061

DOI: 10.1002/adma.202405061

O. J. Sandberg
Physics
Faculty of Science and Engineering
Åbo Akademi University
Turku 20500, Finland

S. Gielen, W. Maes
Institute for Materials Research (IMO)
Hasselt University
Agoralaan 1, Diepenbeek B-3590, Belgium

S. Gielen, W. Maes
IMEC
Associated Lab IMOMEC
Wetenschapspark 1, Diepenbeek B-3590, Belgium

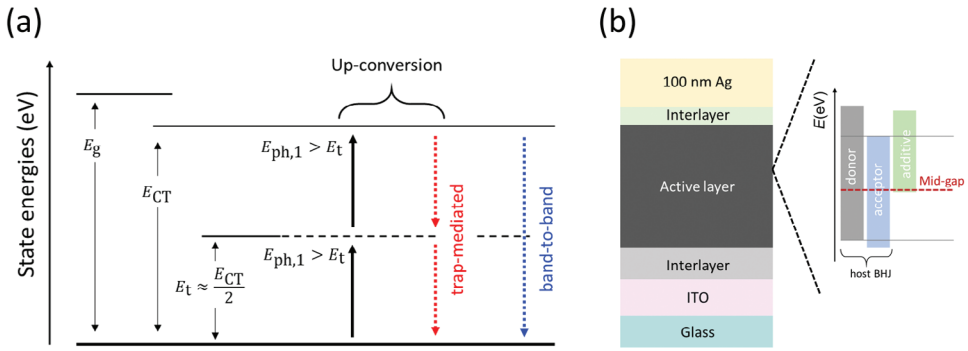

Figure 1. Mid-gap trap states in OPDs and device architecture of trap-doped OPDs investigated in this work. a) State energy diagram and related mid-gap trap state-related parameters in organic donor(D):acceptor(A) systems. The process of photon absorption via the effective gap, charge transfer (CT) state, and mid-gap trap states are indicated by upward arrows; recombination pathways are represented by downward arrows. b) Schematic illustration of the device architecture with relative energy level diagram of the D:A bulk heterojunction (BHJ) host system and organic dopant.

factors such as thermal budget sensitivity, the necessity for large area apertures, cost considerations, or the requirement for lightweight and conformal flexibility.

The photo-active layer of an OPD typically comprises a blend of two organic semiconductors, referred to as the donor (D) and acceptor (A) [respectively the p- and n-type analogues from conventional semiconductor nomenclature], forming a bulk heterojunction (BHJ) photodiode. While the spectral response of OPDs generally depends on the absorption onset of the organic semiconductor component with the smaller optical (excitonic) gap, the noise current is ideally only limited by the energy E_{CT} of D-A charge transfer (CT) states.[13,14] In general, E_{CT} reflects the energy difference between the highest occupied molecular orbital (HOMO) of the donor and the lowest unoccupied molecular orbital (LUMO) of the acceptor. To achieve SWIR or broadband photodetection with OPDs different approaches have been adopted. These include combining near-IR-absorbing (NIR), narrow-gap polymer donors with (non-) fullerene acceptors or dyes,[15–19] implementing (optical) microcavities through optical spacers[20] or fine-tuning of the photo-active layer thickness to enhance light absorption via CT states,[21–24] or utilizing charge-collection narrowing effects via optically and electrically thick junctions.[25,26]

However, several studies have now reported that the performance of OPDs is limited by trap states within the gap.[27–32] The performance-limiting traps were suggested to predominantly be composed of mid-gap states, situated at an energy E_t half of the effective gap ($E_t \approx E_{CT}/2$), and found to be universally present in organic semiconductors.[30] These traps enhance the noise current through their impact on the dark current, which is expected to increase exponentially with decreasing E_{CT}, thus being particularly detrimental in low-gap BHJ systems relevant for SWIR detection. Furthermore, these mid-gap trap states were shown to contribute to both i) free charge carrier generation through a two-step optical release process, referred to as "photo up-conversion" [where a trapped charge is up-converted to a CT state via NIR photons], and ii) subsequent non-geminate (radiative and non-radiative) recombination.[33] **Figure 1a** shows a state energy diagram depicting mid-gap trap state-related processes in an organic semiconductor D:A BHJ system.

Whilst these mid-gap states do ultimately limit the performance (notably D^* via the noise current) in OPDs, especially in systems with small energy gaps, realizing that they seem ubiquitous in disordered semiconductors, one could adopt an approach of utilizing them especially to facilitate a SWIR photo-response. In our current work, we introduce a somewhat counter-intuitive approach of "trap-doping" in BHJs to realize SWIR and broadband OPDs. The trap-doped OPDs are achieved by intentionally incorporating small quantities of a guest organic molecule into a D:A BHJ host system without modifying the thickness of the photo-active layer. More precisely, the HOMO-level energy of the organic additive is situated close to the mid-gap of the D:A host material system, such that the guest molecules will act as partially radiative traps within the D:A gap. Using this approach, we present a proof-of-concept for a VIS-SWIR broadband OPD, demonstrating both specific detectivities exceeding 10^8 Jones and linear dynamic ranges surpassing 100 dB across the entire spectral range from VIS up to sub-1 eV SWIR. Furthermore, we demonstrate that trap-doped OPDs can be utilized to achieve enhanced sub-1 eV SWIR photodetection without simultaneously compromising its performance in the complementary VIS spectrum.

2. Results and Discussion

The OPDs investigated in this work had the following device architecture: Glass | ITO (150 nm) | interlayer | photo-active BHJ layer | interlayer | Ag (100 nm). Detailed information on the device fabrication, chemical definitions and structures of the organic materials along with current density versus voltage curves are provided in Supporting Information. Figure 1b, Supporting Information shows a schematic illustration of the device architecture with the relative energy level diagram of a D:A BHJ host and an organic additive. The trap-doping strategy involves deliberately incorporating small quantities of a guest organic molecule into a D:A BHJ host system without modifying the thickness of the active layer. Provided that the concentration of the additive is small enough such that the embedded organic dopants are well-dispersed within the intermixed D:A matrix to hinder direct charge transport between pure additive sites, the guest molecules will act as partially radiative traps within the D:A gap. Additionally, to achieve enhanced photodetection in the SWIR, the alignment of the additive's HOMO level ($E_{HOMO,additive}$) with the host

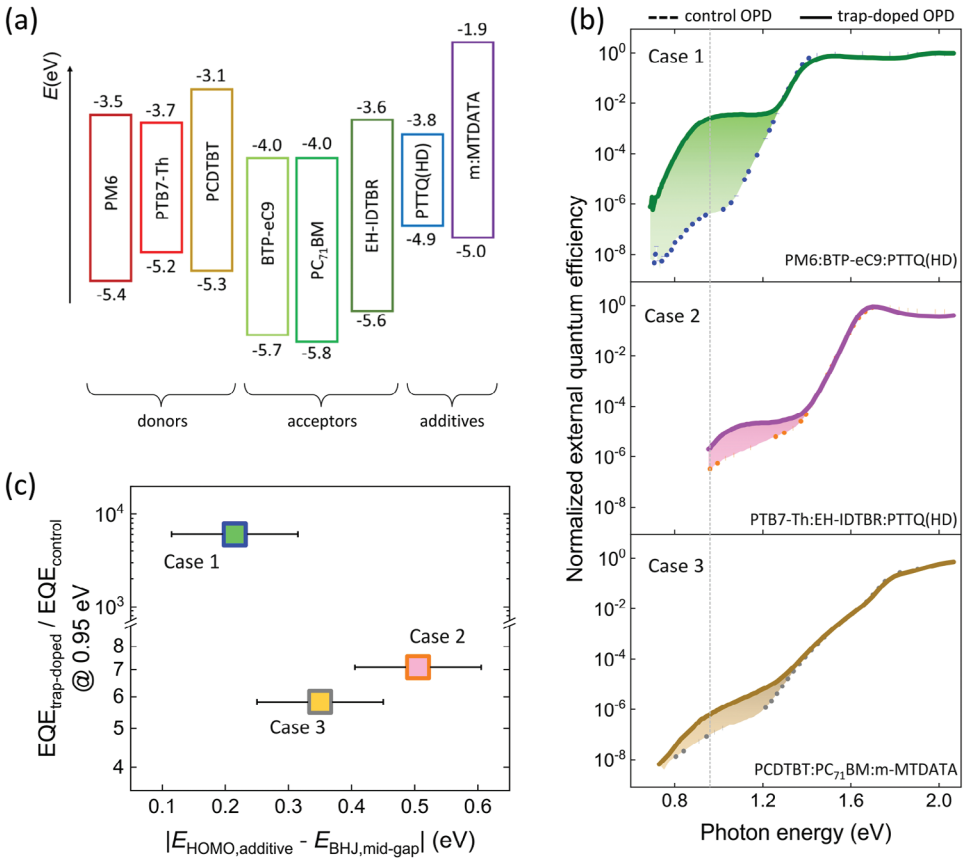

Figure 2. a) Energy levels and external quantum efficiency of trap-doped OPDs. a) HOMO and LUMO energy values, as taken from literature[34–41] of donor, acceptor and additive materials investigated in this works. b) Normalized EQE of (upper panel) PM6:BTP-eC9 without (control; blue) and with (trap-doped; green) the narrow-gap additive PTTQ(HD), (middle panel) PTB7-Th:EH-IDTBR without (control; orange) and with (trap-doped; pink) the additive PTTQ(HD), and (lower panel) PCDTBT:PC71BM without (control; grey) and with (trap-doped; dark yellow) the wide-gap additive m-MTDATA. The colored shaded areas mark the gain in EQE of the trap-doped OPD compared to the control devices. The vertical, grey dotted lines correspond to a photon energy of ≈0.95 eV. c) Calculated ratio of the EQE values at ≈0.95 eV of the trap-doped and control systems from panel (b) plotted against the energetic offset between the corresponding D:A BHJ host's mid-gap and the additive's HOMO energy level. The error bars represent the uncertainty commonly associated with the energy level determination.

D:A BHJ's mid-gap level ($E_{BHJ,mid\text{-}gap}$) serves as a key design metric. The closer $E_{HOMO,additive}$ is to $E_{BHJ,mid\text{-}gap}$, the higher the probability for radiative trap sites to participate in the trap-mediated charge generation of free charge carriers from photons of energy $E_{ph} < E_{CT}$. In this regard, ultra-sensitive external quantum efficiency (EQE) measurements of three different cases were performed: (*Case 1*) a PM6:BTP-eC9 host system with PTTQ(HD) as additive; (*Case 2*) a PTB7-Th:EH-IDTBR host system with PTTQ(HD) as additive; and (*Case 3*) a PCDTBT:$PC_{71}BM$ host system with m-MTDATA as the organic additive. The D:A BHJs and dopants were specifically chosen to present a broad range of energy level alignment between $E_{HOMO,additive}$ and $E_{BHJ,mid\text{-}gap}$ (estimated from the energetic difference between D's HOMO and A's LUMO energy level).

Figure 2a shows the HOMO and LUMO energy values of the D, A, and organic dopant materials; the energy values were extracted from literature using ultraviolet photoelectron spectroscopy (UPS) (for PCDTBT,[34] m-MTDATA,[35] PBT7-Th,[36] PM6,[37] EH-IDTBR,[38] PCBM,[39] and BTP-eC9.[40]) and cyclic voltammetry (CV) (for PTTQ(HD)[41]). The error bars represent the uncertainty in energy level determination in UPS and CV. In Figure 2b, the normalized EQE for host D:A BHJs without (control; dashed lines) and with 1 weight percent (w%) of additives (trap-doped; solid lines) for *Case 1*, *Case 2*, and *Case 3* are shown as a function of photon energy in the upper, middle, and bottom panels, respectively. The ultra-sensitive EQE measurements were conducted at room temperature and over a wide range of photon energies using a home-built EQE apparatus.[42] No bias voltage was applied (i.e., $V_{bias} = 0$ V) Details of the EQE measurements are provided in Supporting Information.

While the below-gap EQE signals (in the SWIR) are attributed to trap-mediated charge generation, the EQE in the VIS region originates from above-gap absorption in the host system, characterized by direct band-to-band transitions leading to relatively high responsivity. Furthermore, the significantly different EQE spectra in the sub-1 eV SWIR regime between *Cases 1–3* are attributed to the differences in the relative energetics expected to critically impact the trap-mediated charge generation. As demonstrated in *Case 1* (upper panel), the introduction of 1 w% of the narrow-gap polymer PTTQ(HD) to the PM6:BTP-eC9 host

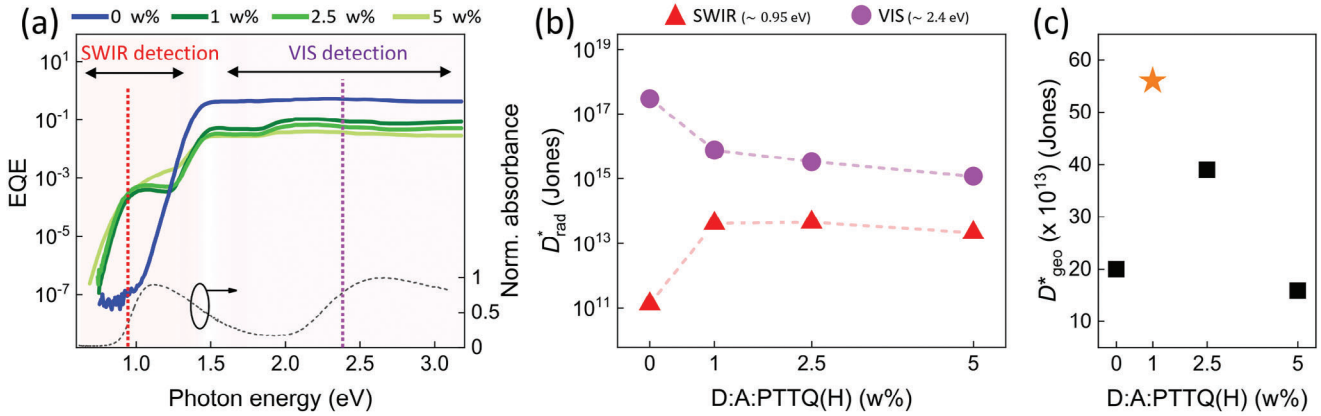

Figure 3. Influence of PTTQ(HD) additive concentration on EQE, upper radiative limit of *D**, and OPD's extent of broadband light sensing. a) EQE (left axis) of a PM6:BTP-eC9:PTTQ(HD) BHJ OPD plotted as a function of photon energy and compared for different concentrations of the narrow-gap polymer additive PTTQ(HD): 0 (control), 1, 2.5, and 5 w%. The red and purple vertical dashed lines mark the photon energy of ≈ 0.95 and ≈ 2.4 eV, respectively, at which the theoretical upper limit of specific detectivity (*D**) in the SWIR and VIS were examined. The normalized absorbance of the neat PTTQ(HD) (right axis) is plotted against the photon energy. b) Upper radiative limit of *D** plotted as a function of PTTQ(HD) additive concentration in the PM6:BTP-eC9 host system and compared in the SWIR (red symbols) and VIS (purple symbols). c) Geometrical mean, as calculated via $D^*_{geo} = \sqrt{D^*_{SWIR} \times D^*_{VIS}}$, plotted against the PTTQ(HD) additive concentration. The star symbol marks the trap-doped OPD with superior D^*_{geo}.

system, where the additive's HOMO level (−4.9 eV) closely aligns with the host D:A BHJ's mid-gap level (−4.7 eV), leads to a significant improvement in SWIR absorption and corresponding sub-gap EQE (see coloured shaded area). In *Case 2* (middle panel), where the PTTQ(HD) additive's HOMO level is more distant from the PTB7-Th:EH-IDTBR host BHJ's mid-gap level (−4.6 eV), a much weaker EQE enhancement is obtained. A similar misalignment is observed for *Case 3* (bottom panel), where the wide-gap additive m-MTDATA, having a HOMO level of about −5.0 eV compared to the PCDTBT:PC_{71}BM host system's mid-gap level of −4.6 eV, results in a much smaller EQE enhancement relative to *Case 1*. In Figure 2c, the calculated ratios of the corresponding EQE values at ≈ 0.95 eV (see vertical grey dotted line in Figure 2b), as a proxy for the degree of trap-doping related SWIR EQE enhancement, of *Cases 1–3* between the trap-doped and control systems are plotted against the energetic offset between $E_{BHJ,mid\text{-}gap}$ and $E_{HOMO,additive}$ in a log-linear plot. In *Case 1*, corresponding to the system with the most pronounced improvement in the SWIR-spectral range EQE, an enhancement of over 3.5 orders of magnitude is observed. As a result, the PM6:BTP:eC9:PTTQ(HD) (1 w%) system emerges as the most promising candidate for achieving enhanced SWIR photodetection and will therefore be the primary focus of further investigation.

To find the optimal concentration of added, radiative mid-gap states at which the SWIR (and broadband) photodetection enhancement is maximized, ultra-sensitive EQE measurements (under short-circuit conditions) were conducted on PM6:BTP-eC9 devices with different concentration of the PTTQ(HD) additive. **Figure** 3a shows the EQE spectra (left axis) of PM6:BTP-eC9 OPDs plotted as a function of photon energy, and compared for 0, 1, 2.5, and 5 w% PTTQ(HD) additive. As shown, the introduction of trace amounts of PTTQ(HD) into the PM6:BTP-eC9 BHJ impacted both the VIS and SWIR spectral regime: While the sub-gap EQE (at ≈ 0.95 eV; see vertical red dashed line) increased by approximately four orders of magnitude from 10^{-7} to 10^{-3}, a tenfold drop in the related VIS-regime EQE (at ≈ 2.4 eV; see vertical purple dashed line) was observed. The exact EQE values at 520 and 1310 nm are provide in Table S1, Supporting Information. As evident from the normalized absorption spectrum of neat PTTQ(HD) (Figure 3a, right axis), indicating a strong absorption peak ≈1.1 eV, the increase in sub-gap EQE can be attributed to charge carrier generation via the narrow-gap polymer additive (see also Figure S3, Supporting Information). The reduced EQE in the VIS regime is attributed to a reduction of the charge collection efficiency caused by increased trap-assisted recombination, giving rise to a drastic reduction in the short-circuit current and open-circuit voltage in trap-doped devices measured under artificial 1 sun illumination (see Figure S4, Supporting Information). In the SWIR regime, the reduction in the collection efficiency is overshadowed by the drastic increase in trap-mediated charge generation. Furthermore, the fact that the EQE signal is redshifted suggests that the charge carrier generation in the PM6:BPT-eC9:PTTQ(HD) blends is mediated indirectly via the HOMO level of PTTQ(HD), as opposed to direct photon absorption and charge carrier generation via PTTQ(HD) only.

Next, we calculated the upper limit of *D** and compared it in the SWIR and VIS for each additive concentration. In this regard, *D** can be defined as:

$$D^* = \frac{q\lambda\sqrt{A\Delta f}}{hc} \times \frac{EQE}{i_{noise}} \quad (1)$$

where λ is the wavelength, Δf the frequency bandwidth, h the Planck constant, A the device area, c the speed of light, and i_{noise} denotes the noise current. Note that, when the contribution of the ohmic leakage component (often referred to as shunt current density, J_{sh}) to the dark current density is negligible, i_{noise} in reverse bias can be identified with the dark saturation current density (J_0) which is a native device property:

$$i_{noise} = \sqrt{2qJ_0A\Delta f} \quad (2)$$

An upper limit of D^* can be estimated based on the radiative limit of J_0 which, at small reverse bias, is given by $J_0^{RAD} = q\int_0^\infty EQE(E)\phi_{BB}(E)dE$, where ϕ_{BB} denotes the spectral flux density of the black body spectrum at room temperature. Note that $EQE = EQE_{free} + EQE_{trap}$, accounting for both (i) transitions associated with CT states or excitons (i.e., radiative band-to-band transitions; EQE_{free}), and (ii) radiative transitions taking place via mid-gap trap states (EQE_{trap}).[43] Figure 3b shows the calculated upper radiative limit of the specific detectivity (D^*_{rad}) based on J_0^{RAD}, as obtained from the integrated EQE, plotted against the concentration of PTTQ(HD) additive, and compared in the SWIR spectral range at ≈ 0.95 eV (D^*_{SWIR}; red symbols) and in the VIS spectral range at ≈ 2.4 eV (D^*_{VIS}; purple symbols). Here, two observations can be made: (i) the introduction of PTTQ(HD) results in a significant decrease (increase) in D^*_{VIS} (D^*_{SWIR}) by approximately two (three) orders of magnitude, and (ii) whilst the change in D^*_{SWIR} across the different PTTQ(HD) concentrations is relatively negligible (amounting to roughly 3.6×10^{13} Jones), a noticeable drop in D^*_{VIS} from ≈ 7.6×10^{15} Jones (1 w%) down to ≈ 1.2×10^{15} Jones (5 w%) is observed. We note that the introduction of the additional trap states will increase the shot noise (see Equation 2). However, since the shot noise will scale by $\sqrt{EQE_{SWIR}}$, D^* in the SWIR regime will increase by $\sqrt{EQE_{SWIR}}$ (see Equation 1) leading to a net improvement in detectivity of trap-doped OPDs. We want to emphasize that the calculated values of D^*_{VIS} and D^*_{SWIR} in Figure 3b exclusively represent the upper theoretical limits, disregarding non-radiative loss mechanisms and any additional noise sources beyond shot noise. In this sense, these limits represent the art-of-the-possible using the trap-doping mechanism. Figure 3c shows the calculated geometrical mean, $D^*_{geo} = \sqrt{D^*_{SWIR} \times D^*_{VIS}}$ (relevant to exponentially different values), as a proxy to assess a photodetector's extent of broadband light sensing, plotted as a function of additive concentration. As shown, D^*_{geo} is maximized for the PM6:BTP-eC9 system with 1 w% of PTTQ(HD) (see star symbol in Figure 3c).

Having established the additive concentration for enhanced SWIR and broadband photodetection, we next characterized the photodetector performance of the PM6:BTP-eC9:PTTQ(HD) (1 w%) trap-doped OPD. To this end, we first examined the linear dynamic range (LDR) – a quantity providing information about a photodetector's range of linear photocurrent-to-incident light intensity behavior – of the trap-doped OPD in the VIS and SWIR spectral range and compared it to the control PM6:BPT-eC9 OPD. **Figure 4a** shows the normalized EQE of the control (blue) and trap-doped (green) OPD (under short-circuit conditions) plotted as a function of photon energy; the red and purple dashed lines mark the SWIR (i.e., $\lambda_{exc} = 1310$ nm, or ≈ 0.95 eV) and VIS (i.e., $\lambda_{exc} = 520$ nm, or ≈ 2.4 eV) laser excitation wavelengths, respectively, at which the corresponding SWIR- and VIS-LDRs were examined. Note that the measurements were carried out in both *ac*- and *dc*-mode; technical details of the experimental setup are provided in Supporting Information.

Figure 4b shows the photocurrent (at $V_{bias} = 0$ V) of the control (blue symbols) and trap-doped (green symbols) OPD plotted as a function of incident light intensity at an excitation wavelength of $\lambda_{exc} = 1310$ nm; square (star) symbols refer to the *dc*-(*ac*-) mode measurements. While the horizontal lines mark the noise floors, black dashed lines are guides to the eye corresponding to a unity slope. The noise floors were determined from the noise spectral density (NSD) spectra of the corresponding OPDs (see Figure S1, Supporting Information); details are provided in Supporting Information. It is expected that the noise current level associated with traps in the trap-doped device is higher as compared to the control OPD. However, a noise floor of $i_{noise} \approx 4.3 \times 10^{-14}$ A and $i_{noise} \approx 4.5 \times 10^{-14}$ A for the control and trap-doped OPD were determined, respectively, implying a similar D^*_{rad} (see Equation 1). The similarity in determined noise current suggests that the noise in both devices is dominated by thermal noise from external shunt effects (induced by non-idealities in device structure) rather than by the internal noise of the diodes themselves. As shown in Figure 4b, both OPDs show a linear photocurrent-to-light power response in the probed intensity range indicative of the absence of higher-order photocurrent loss mechanisms (e.g., bimolecular recombination).[44] From the intersect of noise floor and unity slope, the noise equivalent power (NEP) was quantified, and found to be $NEP_{control} \approx 2.3 \times 10^{-6}$ $WHz^{-1/2}$ and $NEP_{trap\text{-}doped} \approx 5.7 \times 10^{-10}$ $WHz^{-1/2}$. The specific detectivity, as calculated via $D^* = \sqrt{A}/NEP$, of the control OPD amounted to $D^*_{control} \approx 8.7 \times 10^4$ Jones, which increased by roughly three orders of magnitude to $D^*_{trap-doped} \approx 3.6 \times 10^8$ Jones for the trap-doped device – a value that is close to state-of-the art SWIR OPDs, with reported values approaching specific detectivities of ≈10^9 −10^{10} Jones at 0.95 eV.[16,17,45] Based on the ratio of maximum device photocurrent density, J_{max} (i.e., the current associated with the light power at which bimolecular recombination initiates), and minimum current density (i.e., noise floor), J_{min}, the LDR for the probed intensity range was calculated via $LDR = 20\log(J_{max}/J_{min})$. Whilst the control device shows an LDR in the SWIR of 40 dB, the trap-doped OPD demonstrates a significant |60 dB| boost to ≈110 dB.

Figure 3c is a repetition of panel (b), but plotted for the VIS excitation wavelength. **Table 1** summarizes the determined i_{noise}, NEP, and D^* for both the control and trap-doped OPD at $\lambda_{exc} = 520$ nm and $\lambda_{exc} = 1310$ nm. It is noteworthy that D^*, NEP, and i_{noise}, as acquired for the VIS spectral range, exhibit striking similarities between the two systems, confirming no drastic deficiency in the photodetector performance within the VIS spectral range subsequent to trap-doping.

Our proof-of-concept VIS-SWIR trap-doped OPD is partially approaching, if not surpassing, the performance metrics of state-of-the-art broadband OPDs in certain photodetector performance parameters, such as D^* or LDR. Here, it is important to note that making a direct comparison of these performance parameters can be challenging due to different measurement conditions (e.g., probing the LDR under different electrical and light biasing conditions) and calculation methods (e.g., determining D^* based on NEP, i_{noise}, or the dark current). In light of these challenges, Jacoutot et al. reported on an ultra-low bandgap polymer/non-fullerene acceptor OPD that detects SWIR light up to 1800 nm, exhibiting D^* values ranging between ≈$10^8$and 10^{10} Jones (at $V_{bias} = -2$ V) and thereby yielding slightly higher specific detectivities compared to our trap-doped OPD.[16] However, they determined much lower LDRs of merely 50 dB in the VIS and SWIR when compared to the $LDR_{VIS} \approx 220$ dB and $LDR_{SWIR} \approx 110$ dB achieved in our trap-doped OPD. While there are

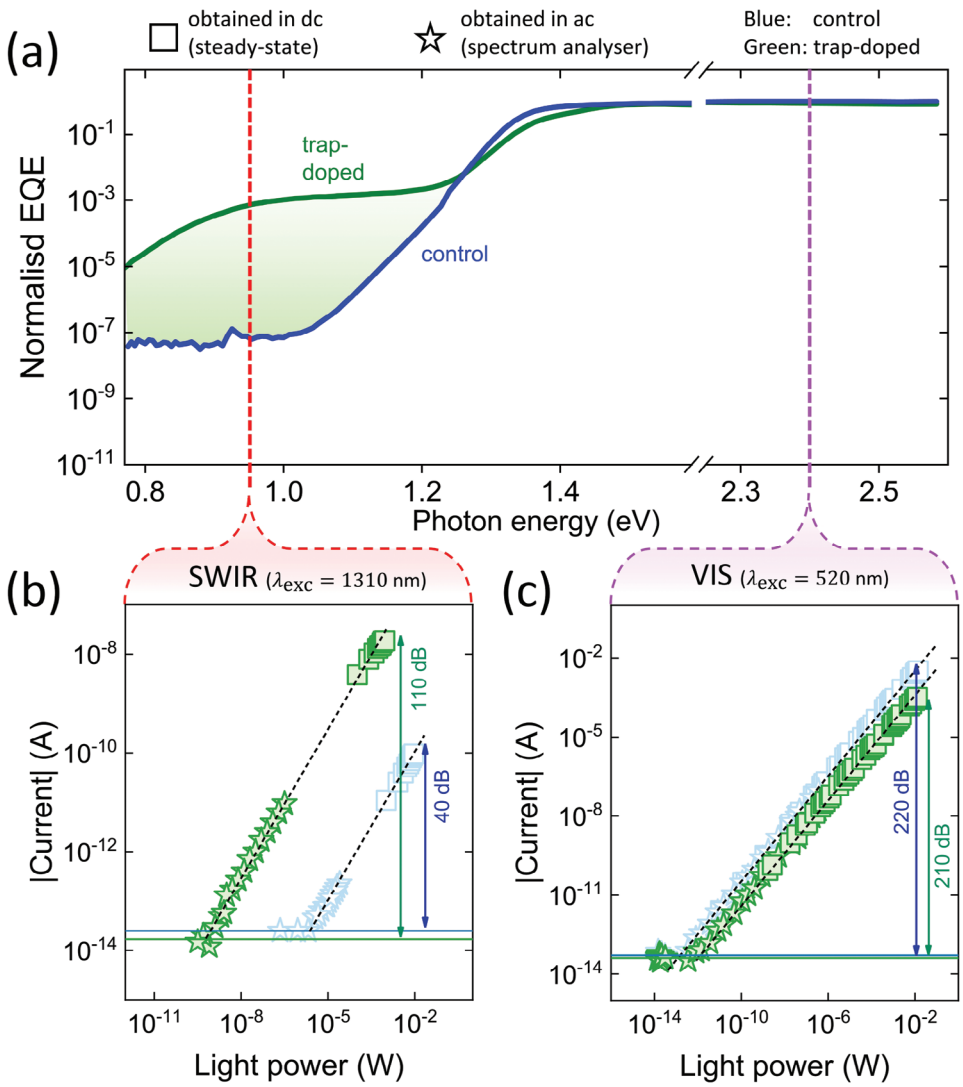

Figure 4. Linear dynamic range: enhanced SWIR and broadband light sensing performance upon trap-doping. a) Normalized EQE plotted as a function of photon energy and compared between the 220 nm thick control (blue solid line) and 1 w% PTTQ(HD) trap-doped (green solid line) OPD. The purple (red) vertical dashed line marks the VIS- (SWIR-) laser excitation wavelength at 520 nm (1310 nm). b) Photocurrent of the control (blue) and trap-doped (green) OPD plotted against the incident light intensity at a laser excitation wavelength of 1310 nm. While square (star) symbols correspond to data as obtained in *dc*-(*ac*-) mode, blue and green horizontal lines mark the noise floor of the control and trap-doped OPD, respectively. Furthermore, black dashed lines are guides to the eye with a slope of 1 AW^{-1}. c) Repetition of panel (b) but plotted for a laser excitation wavelength of 520 nm.

Table 1. Photodetector broadband light-detection performance parameters. Calculated specific detectivity (D^*) and Noise equivalent power (NEP), and measured noise floor (i_{noise}) along with their estimated standard deviations, as obtained for the control and trap-doped OPDs, compared at different laser excitation wavelengths (λ_{exc}).

OPD	λ_{exc} in [nm]	D^* in [Jones]	NEP in [$WHz^{-1/2}$]	i_{noise} in [A]
Control	520	$(1.5 \pm 0.1) \times 10^{12}$	$1.3 \times 10^{-13} \pm 9.5 \times 10^{-15}$	$(4.3 \pm 1) \times 10^{-14}$
	1310	$(8.7 \pm 0.5) \times 10^{4}$	$2.3 \times 10^{-6} \pm 9.5 \times 10^{-15}$	$(4.3 \pm 1) \times 10^{-14}$
trap-doped	520	$(2.6 \pm 0.2) \times 10^{11}$	$7.5 \times 10^{-13} \pm 8.9 \times 10^{-15}$	$(4.5 \pm 0.9) \times 10^{-14}$
	1310	$(3.6 \pm 0.2) \times 10^{8}$	$5.7 \times 10^{-10} \pm 8.9 \times 10^{-15}$	$(4.5 \pm 0.9) \times 10^{-14}$

additional reports demonstrating SWIR broadband OPDs achieving high specific detectivities (under reverse bias voltages) ranging from 10^9 to even 10^{11} Jones for SWIR wavelength up to 1500 nm, these reports, however, lack in the measurement and provision of corresponding LDR values.[17,46]

We note that recent studies have shown EQE values ≈0.2% at 1300 nm and dark currents as low as $2.52 \pm 0.19 \times 10^{-10}$ A cm^{-2} for a SWIR-OPD based on PCE10:BDP4C.[18] Tsai et al. achieved EQEs of ≈3% (up to 30% at −4 V reverse bias) for SWIR-OPDs using a cross-linkable naphthalenediimide derivative as electron transport layer.[47] Furthermore, Luong et al. reported LDRs of up to 144 dB at 1085 nm excitation wavelength for resonant-cavity enhanced PTB7-Th:COTIC-4F OPDs,[48] while Yin et al. achieved detectivities exceeding 10^{12} Jones at 1300 nm under zero bias voltage.[49]

Finally, we want to highlight that, although currently conceptual and aimed at SWIR and broadband photo-detection, we believe our trap-doping approach may have broader applications across different spectral windows. In this regard, the selectivity of the spectral window and the extent of broadband light sensing of trap-doped OPDs are speculated to be influenced by factors such as absorption onset of the D:A host system, the specific energetics of the mid-gap states, and the proper integration of trace amounts of organic guest molecules into the D:A BHJ host system.

3. Conclusion

In conclusion, we introduced the somewhat counter-intuitive approach of trap-doping in BHJ OPDs to achieve SWIR and broadband photodetection. This approach leverages ubiquitous mid-gap states in disordered semiconductors to specifically enhance the SWIR photo-response. We presented a proof-of-concept for a VIS-SWIR broadband OPD that shows specific detectivities in the SWIR spectral range at 0.95 eV and in the VIS spectral range at 2.4 eV, each approximately equal to 10^8 and 10^{12} Jones, respectively. Additionally, the OPD exhibits linear dynamic ranges of 110 dB in the SWIR spectral range and 220 dB in the VIS spectral range. These performance metrics closely approach and even partly surpass those of state-of-the-art VIS-SWIR broadband OPDs. Although the trap-doping approach is currently in the proof-of-concept stage, it shows broad applicability to different spectral windows.

Supporting Information

Supporting Information is available from the Wiley Online Library or from the author.

Acknowledgements

This work was funded through the Welsh Government's Sêr Cymru II Program "Sustainable Advanced Materials" (Welsh European Funding Office—European Regional Development Fund). P.M. is a Sêr Cymru II Research Chair funded through the Welsh Government's Sêr Cymru II "Sustainable Advanced Materials" Program (European Regional Development Fund, Welsh European Funding Office and Swansea University Strategic Initiative). This work was also funded by UKRI through the EPSRC Programme grant EP/T028513/1 Application Targeted Integrated Photovoltaics and the Centre for Integrative Semiconductor Materials (UKRI Research Partnership Investment Fund). S.G. acknowledges the Research Foundation – Flanders (FWO) for granting a junior Post Doc fellowship (1266923N).

Conflict of Interest

The authors declare no conflict of interest.

Author Contributions

A.A. and P.M. provided the overall leadership of the project. A.A., N.Z., and O.J.S. conceptualized the idea. N.Z. and S.Z. designed the experiments. S.Z. and N.Z. performed the measurements. N.Z. fabricated the devices. S.G. assisted in the device fabrication. W.M. provided the narrow-gap materials. N.Z., O.J.S., S.Z., and A.A. interpreted the data. All authors contributed to the development of the manuscript, which was initially drafted by N.Z.

Data Availability Statement

The data that support the findings of this study are available from the corresponding authors upon reasonable request.

Keywords

bulk-heterojunction, mid-gap trap states, organic semiconductors, photodetectors, SWIR, thin films, up-conversion

Received: April 8, 2024
Revised: June 19, 2024
Published online: July 23, 2024

[1] Z. Guo, S. Park, J. Yoon, I. Shin, *Chem. Soc. Rev.* **2014**, *43*, 16.
[2] Y. Xia, C. Geng, X. Bi, M. Li, Y. Zhu, Z. Yao, X. Wan, G. Li, Y. Chen, *Adv. Opt. Mater.* **2023**, *12*, 2301518.
[3] G. Simone, D. Di Carlo Rasi, X. de Vries, G. H. L. Heintges, S. C. J. Meskers, R. A. J. Janssen, G. H. Gelinck, *Adv. Mater.* **2018**, *30*, 1804678.
[4] Q. Lin, A. Armin, P. L. Burn, P. Meredith, *Nat. Photonics* **2015**, *9*, 687.
[5] A. Pierre, A. Gaikwad, A. C. Arias, *Nat. Photonics* **2017**, *11*, 193.
[6] Q. Li, Y. Guo, Y. Liu, *Chem. Mater.* **2019**, *31*, 6359.
[7] A. Ren, H. Wang, W. Zhang, J. Wu, Z. Wang, R. V. Penty, I. H. White, *Nat. Electron.* **2021**, *4*, 559.
[8] J. Clark, G. Lanzani, *Nat. Photonics* **2010**, *4*, 438.
[9] M. Babics, H. Bristow, W. Zhang, A. Wadsworth, M. Neophytou, N. Gasparini, I. McCulloch, *J. Mater. Chem. C* **2021**, *9*, 2375.
[10] Y. Wei, H. Chen, T. Liu, S. Wang, Y. Jiang, Y. Song, J. Zhang, X. Zhang, G. Lu, F. Huang, Z. Wei, H. Huang, *Adv. Funct. Mater.* **2021**, *31*, 2106326.
[11] P. P. Manousiadis, K. Yoshida, G. A. Turnbull, I. D. W. Samuel, *Philos. Trans. R. Soc. London, Ser. A* **2020**, *378*, 20190186.
[12] F. P. García De Arquer, A. Armin, P. Meredith, E. H. Sargent, *Nat. Rev. Mater.* **2017**, *2*, 16100.
[13] M. Hallermann, S. Haneder, E. Da Como, *Appl. Phys. Lett.* **2008**, *93*, 053307.
[14] A. Armin, W. Li, O. J. Sandberg, Z. Xiao, L. Ding, J. Nelson, D. Neher, K. Vandewal, S. Shoaee, T. Wang, H. Ade, T. Heumüller, C. Brabec, P. Meredith, *Adv. Energy Mater.* **2021**, *11*, 20003570.

[15] Q. Liu, S. Zeiske, X. Jiang, D. Desta, S. Mertens, S. Gielen, R. Shanivarasanthe, H. G. Boyen, A. Armin, K. Vandewal, *Nat. Commun.* **2022**, *13*, 5194.
[16] P. Jacoutot, A. D. Scaccabarozzi, T. Zhang, Z. Qiao, F. Aniés, M. Neophytou, H. Bristow, R. Kumar, M. Moser, A. D. Nega, A. Schiza, A. Dimitrakopoulou-Strauss, V. G. Gregoriou, T. D. Anthopoulos, M. Heeney, I. McCulloch, A. A. Bakulin, C. L. Chochos, N. Gasparini, *Small* **2022**, *18*, 2200580.
[17] N. Li, Z. Lan, Y. S. Lau, J. Xie, D. Zhao, F. Zhu, *Adv. Sci.* **2020**, *7*, 2000444.
[18] M. Yang, B. Yin, G. Hu, Y. Cao, S. Lu, Y. Chen, Y. He, X. Yang, B. Huang, J. Li, B. Wu, S. Pang, L. Shen, Y. Liang, H. Wu, L. Lan, G. Yu, F. Huang, Y. Cao, C. Duan, *Chemistry* **2024**, *10*, 1.
[19] J. He, Z. Wang, Y. Gao, X. Yu, W. Qiao, M. Shao, Z. Li, *Adv. Opt. Mater.* **2024**, *12*, 2301361.
[20] B. Siegmund, A. Mischok, J. Benduhn, O. Zeika, S. Ullbrich, F. Nehm, M. Böhm, D. Spoltore, H. Fröb, C. Körner, K. Leo, K. Vandewal, *Nat. Commun.* **2017**, *8*, 15421.
[21] C. Kaiser, K. S. Schellhammer, J. Benduhn, B. Siegmund, M. Tropiano, O. Zeika, F. Ortmann, P. Meredith, A. Armin, K. Vandewal, *Chem. Mater.* **2019**, *31*, 9325.
[22] Z. Tang, Z. Ma, A. Sánchez-Díaz, S. Ullbrich, Y. Liu, B. Siegmund, A. Mischok, K. Leo, M. Campoy-Quiles, W. Li, K. Vandewal, *Adv. Mater.* **2017**, *29*, 1702184.
[23] S. Xing, V. C. Nikolis, J. Kublitski, E. Guo, X. Jia, Y. Wang, D. Spoltore, K. Vandewal, H. Kleemann, J. Benduhn, K. Leo, *Adv. Mater.* **2021**, *33*, 2102967.
[24] Y. Wang, B. Siegmund, Z. Tang, Z. Ma, J. Kublitski, S. Xing, V. C. Nikolis, S. Ullbrich, Y. Li, J. Benduhn, D. Spoltore, K. Vandewal, K. Leo, *Adv. Opt. Mater.* **2021**, *9*, 2001784.
[25] A. Armin, M. Hambsch, I. K. Kim, P. L. Burn, P. Meredith, E. B. Namdas, *Laser Photonics Rev.* **2014**, *8*, 924.
[26] A. Armin, R. D. Jansen-Van Vuuren, N. Kopidakis, P. L. Burn, P. Meredith, *Nat. Commun.* **2015**, *6*, 6343.
[27] J. Kublitski, A. Hofacker, B. K. Boroujeni, J. Benduhn, V. C. Nikolis, C. Kaiser, D. Spoltore, H. Kleemann, A. Fischer, F. Ellinger, K. Vandewal, K. Leo, *Nat. Commun.* **2021**, *12*, 551.
[28] G. Simone, M. J. Dyson, C. H. L. Weijtens, S. C. J. Meskers, R. Coehoorn, R. A. J. Janssen, G. H. Gelinck, *Adv. Opt. Mater.* **2020**, *8*, 1901568.
[29] S. Zeiske, O. J. Sandberg, N. Zarrabi, W. Li, P. Meredith, A. Armin, *Nat. Commun.* **2021**, *12*, 3603.
[30] O. J. Sandberg, C. Kaiser, S. Zeiske, N. Zarrabi, S. Gielen, W. Maes, K. Vandewal, P. Meredith, A. Armin, *Nat. Photonics* **2023**, *17*, 368.
[31] X. Ma, R. A. J. Janssen, G. H. Gelinck, *Adv. Mater. Technol.* **2023**, *8*, 2300234.
[32] X. Ma, R. Ollearo, B. T. van Gorkom, C. H. L. Weijtens, M. Fattori, S. C. J. Meskers, A. J. J. M. van Breemen, R. A. J. Janssen, G. H. Gelinck, *Adv. Funct. Mater.* **2023**, *33*, 2304863.
[33] N. Zarrabi, O. J. Sandberg, S. Zeiske, W. Li, D. B. Riley, P. Meredith, A. Armin, *Nat. Commun.* **2020**, *11*, 5567.
[34] E. L. Ratcliff, J. Meyer, K. X. Steirer, N. R. Armstrong, D. Olson, A. Kahn, *Org. Electron.* **2012**, *13*, 744.
[35] S. hun Lee, T. J. Kim, E. Lee, D. Kwon, J. Kim, J. Joo, *Nat. Commun.* **2023**, *14*, 7190.
[36] S. Zhang, L. Ye, W. Zhao, D. Liu, H. Yao, J. Hou, *Macromolecules* **2014**, *47*, 4653.
[37] T. Wang, Z. H. Chen, J. W. Qiao, W. Qin, J. Q. Liu, X. Z. Wang, Y. J. Pu, H. Yin, X. T. Hao, *ACS Appl. Mater. Interfaces* **2023**, *15*, 12109.
[38] J. Bertrandie, J. Han, C. S. P. De Castro, E. Yengel, J. Gorenflot, T. Anthopoulos, F. Laquai, A. Sharma, D. Baran, *Adv. Mater.* **2022**, *34*, 2202575.
[39] B. Walker, A. B. Tamayo, X. D. Dang, P. Zalar, J. H. Seo, A. Garcia, M. Tantiwiwat, T. Q. Nguyen, *Adv. Funct. Mater.* **2009**, *19*, 3063.
[40] J. Wang, Z. Zheng, P. Bi, Z. Chen, Y. Wang, X. Liu, S. Zhang, X. Hao, M. Zhang, Y. Li, J. Hou, *Natl. Sci. Rev.* **2023**, *10*, nwad085.
[41] F. Verstraeten, S. Gielen, P. Verstappen, J. Raymakers, H. Penxten, L. Lutsen, K. Vandewal, W. Maes, *J. Mater. Chem. C* **2020**, *8*, 10098.
[42] S. Zeiske, C. Kaiser, P. Meredith, A. Armin, *ACS Photonics* **2019**, *7*, 256.
[43] N. Zarrabi, O. J. Sandberg, P. Meredith, A. Armin, *J. Phys. Chem. Lett.* **2023**, *14*, 3174.
[44] S. Zeiske, W. Li, P. Meredith, A. Armin, O. J. Sandberg, *Cell Rep. Phys. Sci.* **2022**, *3*, 101096.
[45] T. Yang, K. Sun, X. Liu, W. Wei, T. Yu, X. Gong, D. Wang, Y. Cao, *J. Phys. Chem. C* **2012**, *116*, 13650.
[46] L. Zheng, T. Zhu, W. Xu, L. Liu, J. Zheng, X. Gong, F. Wudl, *J. Mater. Chem. C* **2018**, *6*, 3634.
[47] K. W. Tsai, M. H. Chen, G. Suthar, Y. T. Hsiao, L. C. Cheng, C. Y. Liao, F. C. Chen, C. W. Chu, Y. M. Chang, *Adv. Opt. Mater.* **2024**, *12*, 2302435.
[48] H. M. Luong, C. Kaiyasuan, A. Yi, S. Chae, B. M. Kim, P. Panoy, H. J. Kim, V. Promarak, Y. Miyata, H. Nakayama, T. Q. Nguyen, *ACS Energy Lett.* **2024**, *9*, 1446.
[49] B. Yin, X. Zhou, Y. Li, G. Hu, W. Wei, M. Yang, S. Jeong, W. Deng, B. Wu, Y. Cao, B. Huang, L. Pan, X. Yang, Z. Fu, Y. Fang, L. Shen, C. Yang, H. Wu, L. Lan, F. Huang, Y. Cao, C. Duan, *Adv. Mater.* **2024**, *36*, 2310811.